Surrogate measurement of chlorine concentration on steel surfaces by alkali element detection via laser-induced breakdown spectroscopy

X. Xiao[a], S. Le Berre[a], K.C. Hartig[a], A.T. Motta[a], I. Jovanovic[a, b, *]

[a]Department of Mechanical and Nuclear Engineering, The Pennsylvania State University, University Park, PA 16802, United States
[b]Department of Nuclear Engineering and Radiological Sciences, University of Michigan, Ann Arbor, MI 48109, United States

ARTICLE INFO

ABSTRACT

Chlorine can play an important role in the process of stress corrosion cracking of dry cask storage canisters for used nuclear fuel, which are frequently located in marine environments. It is of significant interest to determine the surface concentration of chlorine on the stainless steel canister surface, but measurements are often limited by difficult access and challenging conditions, such as high temperature and high radiation fields. Laser-induced breakdown spectroscopy (LIBS) could enable chlorine concentration measurements while meeting the other constraints of this application, but suffers from high excitation energy of chlorine and the interference of the atomic emission lines of iron, thus limiting the sensitivity of detection, especially when LIBS has to be delivered over an optical fiber. We demonstrate that chlorine surface concentrations in the range of 0.5–100 mg/m^2 can be inferred by the detection and quantification of sodium contained in chlorine salts if the speciation and neutralization of salts are not of major concern, whereas minor components of sea salt such as magnesium and potassium are less attractive as surrogates for chlorine due to the lower sensitivity of LIBS for their detection and quantification. The limit of detection, measurement accuracy, and other features and limitations of this surrogate measurement approach are discussed.

© 2017 Elsevier B.V. All rights reserved.

1. Introduction

Dry cask storage systems (DCSS) have been designed to provide interim storage of the used nuclear fuel after its cooling in spent fuel pools at nuclear reactor facilities. DCCS have been widely distributed throughout the United States (U.S.) since the first DCCS license was issued by the Nuclear Regulatory Commission in 1986. Currently, there are over 1500 casks at independent spent fuel storage installations licensed to operate in 34 states in the U.S., about one third of which are located in coastal areas. In those circumstances the casks, that comprise stainless steel (SS) canister and steel-lined concrete overpack, can be exposed to salty and humid marine environment, which creates a potential for stress corrosion cracking (SCC) to occur. SCC is a mechanism whereby cracks can propagate even at a stress intensity factor below the critical level in the presence of an attacking environment provided by chlorine (Cl) ions on the surface, sensitized material, and stress. The heat affected zones of welds may experience tensile residual stress, such that the deliquescence of airborne salts that enter through the cask venting systems could help induce SCC of the austenitic SS [1]. Although it can be affected by the environmental conditions, the Cl concentration on the metal structure of the casks is in the range of 1–100 mg/m^2 (0.001–0.1 g/m^2), corresponding to decades of salt deposition, as shown in field tests conducted in Japan [2,3]. Laser-induced breakdown spectroscopy (LIBS) has been reported to be an effective technique for detecting Cl on SS surfaces [2,4]. Features and limitations of this approach must be studied in detail experimentally due to the unique environment in which measurements have to be conducted, which combines the presence of high radiation field, high temperature, and limited access.

LIBS is a method which involves focusing a pulsed laser onto a sample surface to generate a luminous plasma containing ionized and excited particles. Optical emission from the plasma is collected and analyzed spectrally to infer the elemental and isotopic composition of the sample. LIBS has been widely adopted as it enables rapid measurement of trace elements with high spatial resolution and minimal destruction [5–7]. LIBS represents a promising technique for *in-situ* analysis of the concentration of chlorine attached to the SS canister with no need of sample preparation when compared to other traditional *post mortem* methods, such as electric conductivity measurement, atomic absorption spectrometry, and ion

chromatography [2–4]. LIBS can be used to analyze samples with a limited degree of roughness and even with cracks, as long as the sampled spot size is larger than the crack width [8].

The analytical performance of the LIBS technique strongly depends on the choice of experimental parameters, including the laser wavelength and fluence (J/cm^2), pulse duration, pulse shape, ambient gas and pressure, sample surface morphology and temperature, and the detailed geometry of the experimental setup. LIBS has been extensively studied and optimized in the past, such that the limit of detection (LOD) of trace elements has been greatly improved as a result of the significant enhancement of the signal-to-noise ratio of the emission lines [4-7,9-12]. LIBS measurements of Cl attached to SS are challenging due to the high excitation energy of Cl (10.4 eV), low atomization level in the plasma, and the interference of intense atomic emission lines of iron in the region of interest, especially when quantitative concentration measurements are sought at low concentrations and when LIBS has to be delivered over an optical fiber [4,13].

One possible alternative to direct measurement of chlorine is to use the detection of alkali metals as a surrogate to infer the presence of salt (and thus, Cl), assuming that the concentration of these metals is proportional to that of Cl. Prior studies have shown that the ratios of alkali metals, such as Na, Mg, and K, to Cl in most of the oceans and major seas show no significant variation within the limit of analytical error of the ion exchange method [14,15]. However, potential Cl depletion during the transport and deposition of sea salt aerosols in polluted coastal environments and in biogenic sulfuric acid atmosphere could occur as a consequence of pH-lowering reactions with atmospheric acids, leading to the volatilization of Cl as HCl [16,17].

Typical LOD of a few ppm for metallic elements can be achieved in LIBS [18], and if alkali metals are detected at concentrations that suggest the presence of a significant concentration of Cl, more detailed direct measurements of Cl could be performed. In order to use alkali elements as surrogates for Cl, it is necessary to fully understand the transport and deposition mechanism of Cl and alkali elements. It is also necessary to investigate other possible sources of alkali metals such as dust, which could generate false positives. Nevertheless, this measurement approach appears to be a promising path to use LIBS on SS while avoiding the concerns of the interference from Fe, reducing LOD, reducing the laser pulse energy needed for the measurement, reducing the potential detrimental effect of laser ablation, enabling measurements with simpler, single-pulse lasers rather than double-pulse lasers, and enabling fiber-coupled LIBS for field deployment.

In this study, standardized procedures have been developed to prepare samples for LIBS measurements. A nebulizer was used to deposit synthetic seawater on heated (500 K) SS at several Cl surface concentrations below 100 mg/m^2. These samples were analyzed by LIBS at room temperature in air in the wavelength region of Na I, Mg I, K I, and Cl I lines and benchmarked by scanning electron microscopy (SEM), energy dispersive X-ray spectroscopy (EDS), and ion chromatography (IC) techniques. SEM/EDS/IC results and LIBS spectra show high homogeneity achieved in sample preparation, feasibility of quantification of Cl deposited on SS in the concentration range of 0.5–100 mg/m^2 by means of surrogate alkali element measurement in laboratory conditions (primarily by Na and possibly by Mg and K with improved sensitivity), and the practical potential of being integrated into a fiber-coupled LIBS system for application in field environment. Thus, the work presented here will be relevant for measuring and quantifying Cl concentrations if in fact the Na and Cl concentration correlate well (*i.e.* if there is little speciation during transport and deposition on the canisters). Direct LIBS measurement of Cl concentration is also presented to increase the confidence in the results of surrogate measurement, but the high laser intensity on the sample achieved in this open-beam delivery configuration will be difficult to obtain in LIBS with fiber delivery, thus limiting the LOD and even hindering the direct observation of Cl.

2. Experimental setup and methods

In our experiment, a frequency doubled Q-switched Nd:YAG laser (Spectra Physics Quanta-Ray PRO-250-10) with pulse duration of ~10 ns and a repetition rate of 10 Hz was used. The second-harmonic pulses at a wavelength of 532 nm were attenuated to ~40 mJ. Laser pulses were focused using a plano-convex lens with a focal length of 300 mm. The spot diameter on the sample surface, determined by the resulting laser ablation crater shown in SEM results, was approximately 200 μm. A 3-axis travel translation stage was used to provide precise motion control of the sample to expose a "fresh" point on the surface of the sample when requested. Repeated measurements of different spots on the sample surfaces were performed for surface averaging.

As shown in Fig. 1, the light emitted from the plasma was collected in standard atmospheric conditions by a 50-mm focal length lens positioned at 45° with respect to the incident beam for measurement of Na I (589 nm), Mg I (518 nm), and K I (766 nm) emission (collection optics I). The Na I (819 nm) and Cl I (837.6 nm) emission were collected in a coaxial configuration (collection optics II), in which a dichroic mirror passed the 532 nm light and reflected the light with wavelengths greater than 800 nm. A long pass filter with a cutoff near 600 nm was placed in front of the 50 mm collection lens to eliminate the second-order diffraction of the iron lines in the region near 400 nm. The light coupled into the 400-μm diameter quartz fiber was diverted into a Horiba Jobin Yvon iHR550 Czerny-Turner spectrometer with 1200 and 1800 grooves/mm gratings and an Andor iStar 334T intensified charge-coupled device (ICCD). The spectrometer was calibrated using an Ocean Optics DH-2000 light source. A LabVIEW-based data acquisition system was developed to provide proper timing between the mechanical shutter and the ICCD camera through a Stanford Research Systems DG645 delay generator, such that the shutter allowed the desired number of laser shots to pass through and the camera recorded the data with a set gate width and gate delay referenced to the laser pulse. The reported spectra represent an accumulation of two laser ablations for each spot at several different locations spaced at least 1.25 mm apart to account for the transition area of the neighboring spot. The experimental parameters, including the laser pulse energy, the gate delay, and the gate width, were kept identical for analysis of each element, whereas the gain applied to the ICCD was varied and later calibrated.

3. Results and discussion

3.1. Sample preparation and characterization

The standard samples used for calibrating LIBS measurements, *i.e.* determining the relationship between characteristic line emission intensity and areal concentration, were prepared using a PerkinElmer Mira-mist nebulizer (P/N N0775330). Nanoscale aerosol particles were created by the nebulizer by combining the diluted synthetic seawater with an inert gas (argon), which was used as a transporter. The composition of the synthetic seawater is shown in Table 1.

When dried at room temperature (RT), aerosol particles aggregate on the surface of the SS substrates and form crystals much larger than the diameter of the spraying aerosol. More homogeneous salt distribution could be observed when aerosols were deposited on heated (~500 K) surfaces due to the instant vaporization of the water on contact with the surface. A Thermo Scientific Cimarec hot plate was used to preheat the SS substrates. Samples were removed from the hot plate before spraying the salt water because we noticed that the natural convection above the hot plate impacts the salt deposition. The exposure time was limited to 1 min to avoid significant cooling down of the substrates. Reheating of these substrates was
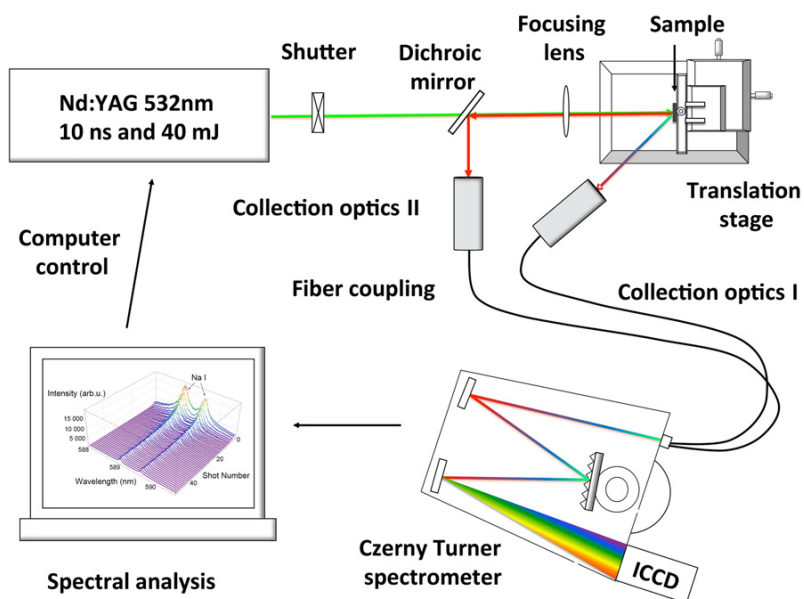
Fig. 1. Experimental setup for LIBS measurement with open-beam delivery.

required for longer spraying time. The experimental setup for sample preparation is shown in Fig. 2.

Two sets of samples (25×25 mm^2) with Cl surface concentration of 0.5–100 mg/m^2 and 2.5–25 mg/m^2 were prepared. These concentrations were calculated from the concentration of the diluted seawater solution, the known well-controlled flow rate of the nebulizer, the exposure time of the samples, and the sprayed sample area. The volumetric flow rate of the nebulizer was 0.25 mL/min. The nebulizer was placed 15 cm above the sample, and the spraying area was measured to be 16 cm^2. The dilution factor was selected to be 1/100, except for the concentrations of 0.5 mg/m^2 and 1 mg/m^2, where a 1/1000 dilution factor was used.

Fig. 3 shows the SEM images taken from samples prepared in this fashion. At RT we observe salt crystals with an average diameter of ~50 μm uniformly spread over the SS substrate at Cl concentration of 3 g/m^2 (Fig. 3 (a)), whereas a continuous film of salt is observed on the heated 100 mg/m^2 substrate, as shown in Fig. 3 (b). Fig. 3 (b–e) shows the salt distribution for Cl concentrations spanning two orders of magnitude, from 5 mg/m^2 to 100 mg/m^2. The salt deposit patterns on the lower concentration samples are regular and form shapes corresponding to the spraying pattern of the nebulizer. The homogeneity of salt concentration over the scale of the focal spot

size and relative salt concentrations of the samples were confirmed using EDS. The samples prepared using the nebulizer show higher homogeneity than the liquid-dried samples and thus have been chosen to serve as standards for LIBS measurements.

A typical area affected by laser ablation on a sample with 25 mg/m^2 Cl concentration can be seen in Fig. 3 (f). The ablation crater geometry was very reproducible from shot to shot. The 200 μm diameter crater is directly surrounded by a depleted area ~600 μm in diameter, on which no salt is detected by EDS, and by a thermally affected area of ~6 mm diameter, in which the salt layer is visibly modified, probably due to melting under the high substrate temperature induced by the deposition of the laser energy. EDS analysis also showed that the salt concentration in the thermally affected area shown in Fig. 3 (f) was not different from that of the unperturbed salt layer. A transition area of ~1.25 mm diameter is observed between the depleted and thermally affected areas, within which a gradient of concentration could be measured. This led us to set the spacing between the measured spots to be at least 1.25 mm, so that each new measurement is made outside

Table 1

Composition of synthetic seawater (Lake Products Company LLC).

Components	Concentration (g/L)
NaCl	24.53
MgCl$_2$	5.20
Na$_2$SO$_4$	4.09
CaCl$_2$	1.16
KCl	0.695
NaHCO$_3$	0.201
KBr	0.101
H$_3$BO$_3$	0.027
SrCl$_2$	0.025
NaF	0.003
Total	36.032
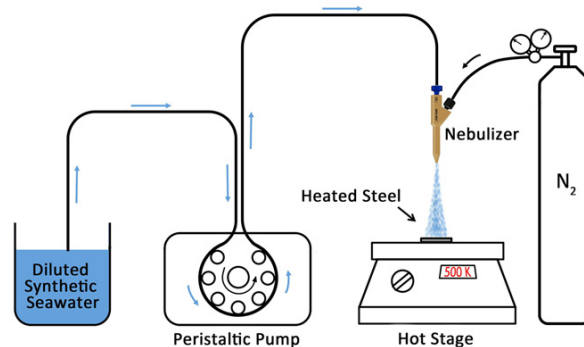
Fig. 2. Experimental setup for sample preparation using PerkinElmer Mira Mist nebulizer (P/N:N0775330).
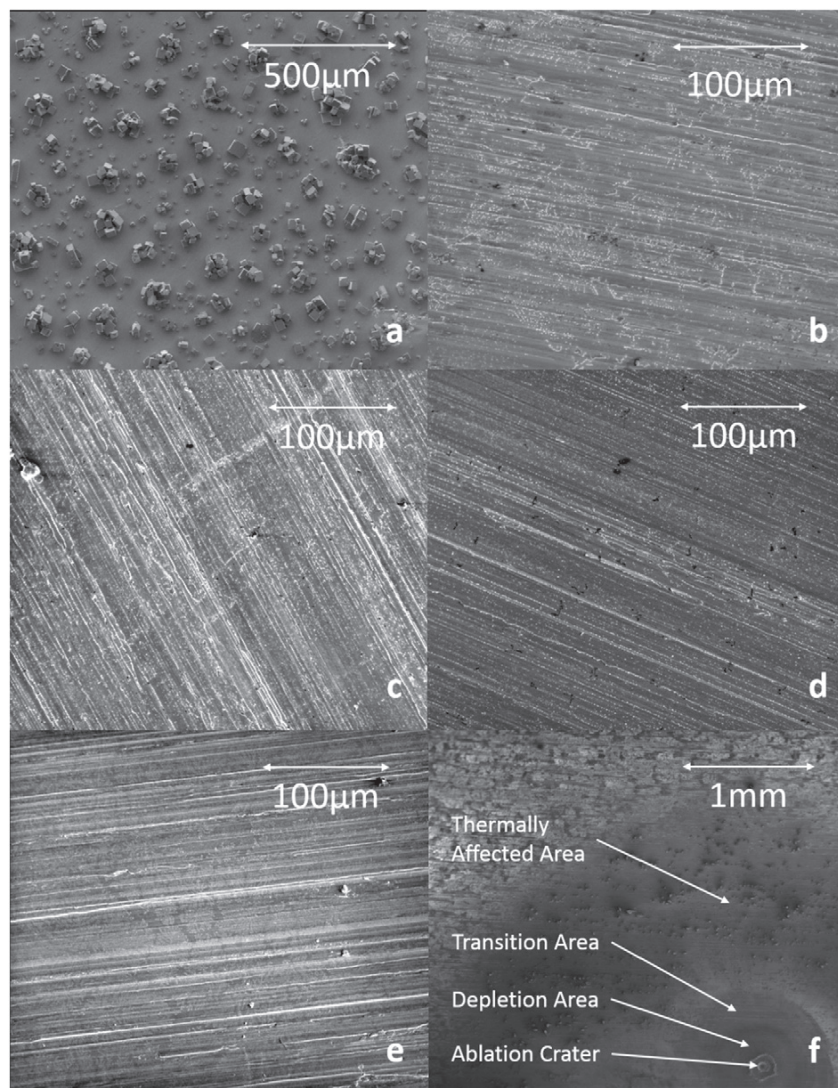
Fig. 3. SEM images of prepared samples: (a) unheated 3 g/m^2; (b) heated 100 mg/m^2; (c) heated 50 mg/m^2; (d) heated 25 mg/m^2; (e) heated 5 mg/m^2; (f) The various affected areas in the vicinity of the ablation spot (FESEM: NanoSEM 630).

of the transition area of prior laser ablations and the concentration of Cl is not affected at the position of the new laser plasma.

Surface concentrations in Cl and alkali elements were first investigated using SEM-EDS to characterize their homogeneity and the composition of salt layers (constant stoichiometry between Cl and Na). To confirm the absolute concentrations, we used ion chromatography (IC), which is a quantitative measurement method for anions in liquid phase. After sample preparation, samples from a given batch were immersed into deionized water inside a micro-cleanser to dissolve their salt layer. The liquid solution was then analyzed with ion chromatography to obtain the surface concentrations. Fig. 4 shows the results we obtained for samples with chlorine concentrations in the range of 0.7–140 mg/m^2. The good agreement between the calculated and the experimentally measured chlorine concentration confirms that calculated concentrations are indeed representative of actual concentrations.

3.2. Spectral analysis for quantification of sea salt concentration on stainless steel

3.2.1. Na I emission line at 589 nm

Fig. 5 (a) shows the Na emission spectra in the spectral range of 587.0–591.5 nm at Na concentrations of 0.28–55 mg/m^2, corresponding to Cl concentration of 0.5–100 mg/m^2. Spectral emission of the hyperfine-split Na D lines at 589.0 nm (D$_2$ line: $3p^2P^o_{3/2} \rightarrow 3s^2S_{1/2}$) and 589.6 nm (D$_1$ line: $3p^2P^o_{1/2} \rightarrow 3s^2S_{1/2}$) has been measured with a gate delay and a gate width time of the ICCD camera of 1 μs and 0.1 μs, respectively, to avoid strong self-reversal effect and alleviate spectral line broadening of Na emissions. The doublet peaks increase and broaden with the increase of Na concentration, indicating an increased electron density and temperature. No significant environmental background Na emission could be detected from the spectrum measured on a blank SS substrate. The emission spectra
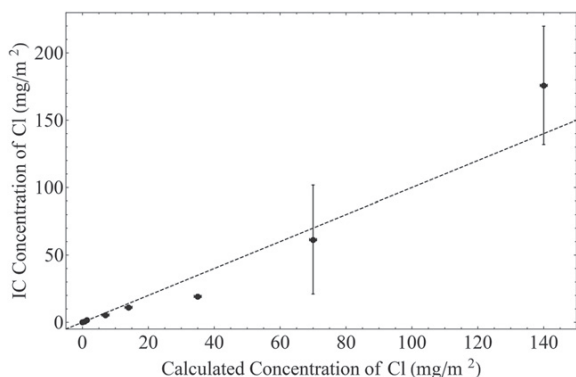
Fig. 4. Dependence of the Cl concentration measured by ion chromatography (IC) on the calculated Cl concentration in the range of 0.7–140 mg/m². The dashed line represents a perfect agreement between the calculated and the measured Cl concentration, whereas the solid circles are the experimental data. The vertical error bars represent the standard deviation of the Cl concentration measured by IC with two sets of samples. The horizontal error bars originate from 3-s timing uncertainty in the sample preparation process.

were averaged over 20 different locations of the sample with accumulation of two laser pulses on each spot. Multiple peak fitting with Lorentz distributions were used for spectral analysis. The Na D_2 line was used for quantification.

The dependence of the emission intensity of the Na D_2 line on calculated Na concentration in the range of 0.28–55 mg/m² is shown in Fig. 5 (b). An exponential relationship is fitted between the calculated Na concentrations and the mean values of intensity of the D_2 line to account for self-absorption of Na I emission [2]. The self-absorption effect is prominent for the Na D lines when the plasma is optically thick, which not only reduces the peak intensity, but also causes the observed line broadening [19]. As a result, the linear dynamic range of this resonance line is limited to $\lesssim$20 mg/m², but it still extends about two orders of magnitude down to 0.28 mg/m² with high sensitivity. The error bars of the Na emission intensity are primarily due to the assumed Gaussian-shaped spraying distribution of the nebulizer and the variability of the emission intensity (error bars of the lowest two data points are too small to be observed in Fig. 5 (b)). The estimated timing uncertainty of 3 s in sample preparation process is the only contribution to the error bars for the calculated concentration. Because of the one order-of-magnitude difference in dilution of the sea salt solution used, data points with Na concentrations below 0.6 mg/m² have a much smaller standard deviation of the calculated concentration of Na; this standard deviation is too small to be displayed in Fig. 5 (b). A good correlation of the measured Na emission intensity with the calculated Na concentration is found with a $R^2 = 0.94$, suggesting that the measurement of Na can be a good surrogate for the measurement of salt concentration in laboratory environment, in which the Cl-to-Na ratio remains approximately constant during the deposition process in sample preparation.

Rapid environmental reactions with atmosphere pollutants, mainly SO_2, H_2SO_4, and HNO_3, may occur during transport and deposition of sea salt aerosol particles, which leads to degassing of HCl and loss of Cl. Consequently, sodium nitrate and sodium sulfate are frequently observed as a surface coating of sea salt particles [16]. The potential change of Cl-to-Na ratio caused by this neutralization of sea salt aerosol particles would compromise the use of alkali elements as surrogates of Cl in LIBS measurements, unless this reaction process is well understood and characterized. In spite of this effect, the surrogate measurement by Na via LIBS technique can still be used to reduce the false negative rates in Cl detection, since it is a much more sensitive approach than the direct measurement of Cl on SS by LIBS.
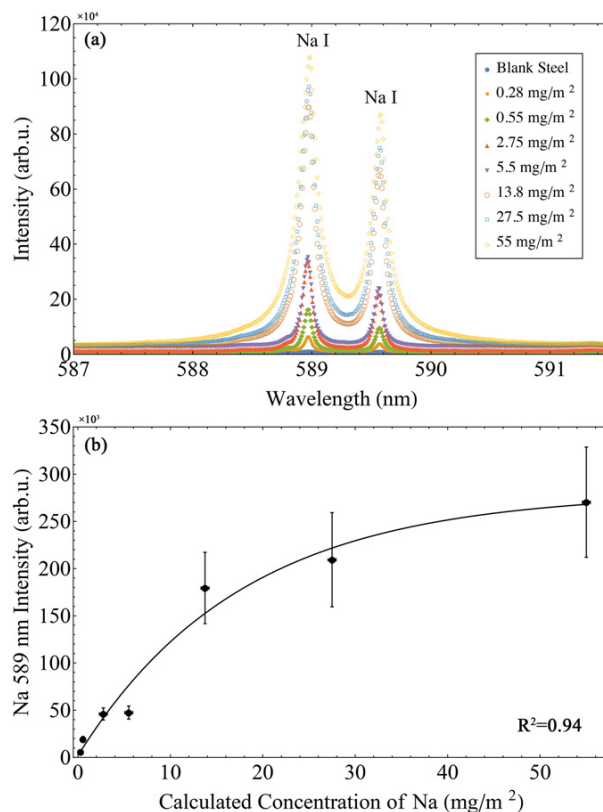
Fig. 5. (a) Na I accumulated emission spectrum (20 position averaged) of SS samples with Na concentrations in the range of 0.28–55 mg/m² and the background spectrum of a blank SS substrate; (b) dependence of the Na I (589.0 nm) emission intensity (peak area) on calculated Na concentration in the range of 0.28–55 mg/m². The corresponding Cl concentration is in the range of 0.5–100 mg/m². The solid line is exponential fit of the experimental data (solid circles). The vertical error bars represent the standard deviation of the emission intensities at 20 positions. The horizontal error bars originate from 3-s timing uncertainty in the sample preparation process. For interpretation of the references to color in this figure legend, the reader is referred to the web version of this article.

This is primarily the result of the low excitation energy of Na and the avoidance of significant interference from the Fe lines. Due to the significant reduction of the required laser intensity, the surrogate LIBS measurement of Cl using Na is desirable for simple fiber delivery configurations and is a promising path for practical use in DCSS.

3.2.2. Other emission lines from Na, K, and Mg

The set of samples used in experiments described in Sections 3.2.2 and 3.2.3 had Cl concentrations in the range of 2.5–25 mg/m². The Na/Cl, Mg/Cl, and K/Cl mass ratios in artificial sea water are 0.55, 0.07, and 0.02, respectively, from which the concentrations of Na, Mg, and K are calculated. We assumed that these ratios were constant during the short transport time in our laboratory environment. The emission spectra of Na I (~819 nm), Mg I (518.4 nm), K I (766.4 nm), and Cl I (837.6 nm) were averaged at five different locations.

Another Na doublet at 818.3 nm $(3d^2D_{3/2} \rightarrow 3p^2P^o_{1/2})$ and 819.5 nm $(3d^2D_{5/2} \rightarrow 3p^2P^o_{3/2})$ have also been measured using a 2-μs gate delay and 10-μs gate width. The Na I line at 819.5 nm was quantified using a Lorentz fit. Fig. 6 (a) shows the calibration curve for the intensity of Na I line at 819.5 nm. This calibration curve is linearly proportional to Na concentration within the range of 0.14–13.8 mg/m². The effect of
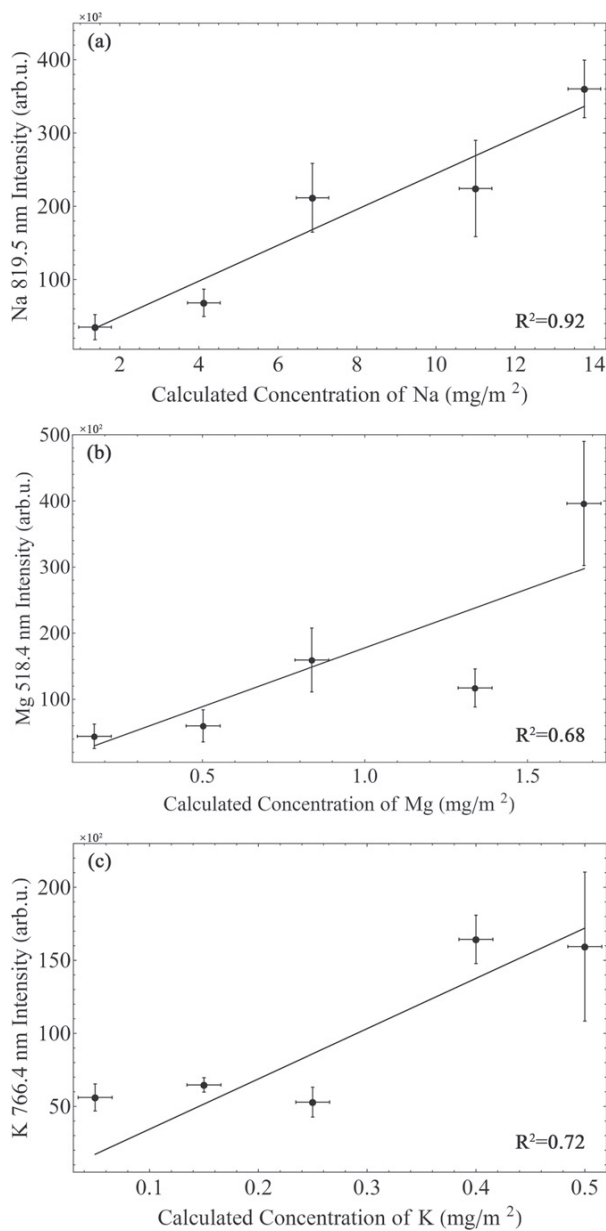
Fig. 6. Dependence of (a) Na I (819 nm) emission intensity (peak area) on calculated Na concentration in the range of 1.4–13.8 mg/m^2; (b) Mg I (518 nm) emission intensity (peak area) on calculated Mg concentration in the range of 0.17–1.67 mg/m^2; (c) K I (766 nm) emission intensity (peak area) on calculated K concentration in the range of 0.05–0.5 mg/m^2. The corresponding Cl concentrations in all plots are 2.5–25 mg/m^2. The solid lines are linear regressions of the experimental data (solid circles). The vertical error bars is the standard deviation of the emission intensities at 5 positions. The horizontal error bars derives from 3-s timing uncertainty in the sample preparation process.

delay of 2 μs and gate width of 10 μs, while for the K I line at 766.4 nm, 0.5-μs delay and 5-μs width were used. Since Mg and K are minor components in the sea salt solution and both emission lines overlap with intense Fe and/or Ar lines, the sensitivity of LIBS based on these surrogate elements is limited. Fig. 6 (b) and (c) shows the dependence of Mg I and K I intensity on the calculated Mg and K concentrations in the ranges of 1.4–13.8 mg/m^2 and 0.05–0.5 mg/m^2, respectively. Relatively poor correlation of the linear fits ($R^2 = 0.68$ for Mg and $R^2 = 0.72$ for K) have been obtained, indicating that the measurement of Mg and K are not the ideal surrogates for the measurement of Cl at such low concentrations in current experimental conditions.

3.2.3. Cl I emission line at 837.6 nm

Fig. 7 (a) shows the emission spectra in which several Cl emission lines belonging to the multiplet of $4p^4D^o \rightarrow 4s^4P$ can be observed in the spectral range of 830.8–844 nm when a gate delay of 0.5 μs and gate width of 5 μs are used. The Cl I line at 837.6 nm ($4p^4D^o_{7/2} \rightarrow 4s^4P_{5/2}$) has the highest intensity and the intensity of this line increases linearly as the concentration of Cl increases from 2.5 mg/m^2 to 25 mg/m^2. Interference from the Fe I line at 838.8 nm, as indicated in the gate width study [4], is no longer a major concern with a higher resolution of the spectrometer used, but the broadened line at
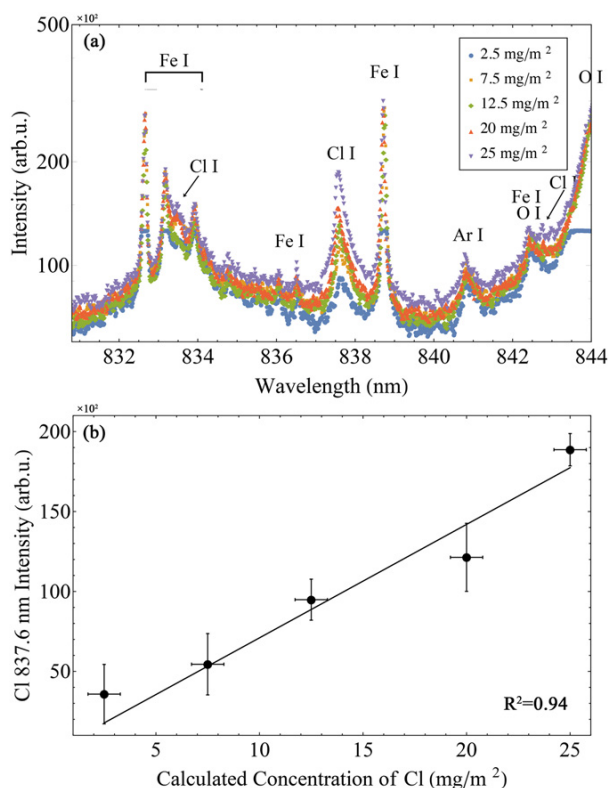
Fig. 7. (a) Cl I accumulated emission spectrum (five position averaged) of the samples at Cl concentration in the range of 2.5–25 mg/m^2; (b) dependence of the Cl I (837 nm) emission intensity (peak area) on the calculated Cl concentration. The solid line is linear regression of the experimental data (solid circles). The vertical error bars represent the standard deviation of the emission intensities at 5 positions. The horizontal error bars originate from 3-s timing uncertainty in the sample preparation process. For interpretation of the references to color in this figure legend, reader is referred to the web version of this article.

self absorption of this Na line is less significant due to the transition to an excited state (3p) and to the low Na concentration. Therefore, a linear model was used to fit the mean Na I emission intensity at 819.5 nm, obtaining a good correlation between the intensity and the concentration with a $R^2 = 0.92$.

Mg and K were investigated as other potential surrogates for Cl measurement. The Mg I line at 518.4 nm was measured using a gate

~837.6 nm is still a result of interference with several Fe emission lines. It can also be seen in Fig. 7 (a) that the intensity of the Fe I lines from the laser-ablated plasma of the matrix and the O I lines from the partial ionization of the air (the most intense Fe I and O I lines at the lowest concentrations were cut off due to saturation of the ICCD camera at high gain) show no significant variation for different Cl concentrations. They could be considered as potential internal standards to reduce the experimental fluctuations of the emission intensity and the matrix effect typical for the LIBS technique [20]. A good linear correlation of the calibration curve with respect to Cl concentration ($R^2 = 0.92$) has been obtained, as shown in Fig. 7 (b).

Although Cl can be directly detected in the current LIBS measurement with open-beam delivery, it is difficult to further reduce the LOD. It is also difficult to conduct direct Cl measurements in the field environment characteristics for DCSS, where fiber transport of a high-power laser pulse is needed. This is because a high laser fluence (at least several J/cm^2) must be used to observe the Cl emission [2]. The input laser energy of even a large-diameter (1 mm) fiber is usually limited to <30 mJ, and the minimum focal spot size that can be obtained following transport through such highly multimode fiber increases linearly with fiber diameter.

On the other hand, quantitative measurement of alkali metals is important not only for the reason that those elements could serve as surrogates for measurement of total Cl concentration if the transport and speciation of salt is fully understood, but also because they indicate the composition of the deposited salt [18,21]. According to Bryan *et al.* [21], the composition of deposits on the SS canister is governed by the rate of deposition and the rate of exchange or reaction with reactive gases in the air, and could vary with location, time, and temperature. This composition determines the temperature and relative humidity at which deliquescence of salt and thus SCC can occur [21]. Further study on the influence of matrix effects also requires the knowledge of deposited salt composition.

4. Conclusion and perspective

Because of the direct LIBS measurement of Cl is complicated by the high excitation energy of Cl which is difficult to reach in LIBS delivered over an optical fiber, we explored the potential for surrogate measurement of Cl in sea salt deposited on SS surfaces by detecting the associated alkali metal Na, and assumed that the ratio of its concentration to that of Cl remains constant during the laboratory sample preparation process. Homogeneous salt deposits with known concentrations on SS substrates were prepared and characterized by SEM/EDS/IC for benchmarking the LIBS measurements. The ability to quantify Cl on SS in concentrations as low as 0.5 mg/m^2 using the Na I line at 589.0 nm has been presented in the laboratory environment. The linear dynamic range of this resonance Na line extends over approximately two orders of magnitude in concentration down to $\lesssim 20$ mg/m^2. Because of the interference with Fe and/or Ar emission lines, K I (766.4 nm) and Mg I (518.4 nm) lines do not show such good correlation between the optical emission intensities and their calculated surface concentrations at corresponding Cl concentrations in the range of 2.5–25 mg/m^2. Samples were also characterized using the Na I line at 819.5 nm and the Cl I line at 837.6 nm with comparable sensitivity with the resonance Na line. Linear relationships between the intensities of Na I (819.5 nm) and Cl I lines and their corresponding concentrations were found. Therefore, we conclude that the LIBS measurement of Na is an effective way of quantifying Cl on SS at low concentrations (as low as 0.5 mg/m^2) if the speciation and neutralization of salts are not of major concern, and may be a promising approach toward fiber-coupled LIBS for deployment in field conditions. Although there is a potential for the Na-to-Cl ratio to be altered in the transport to DCSS, the method could still reduce

the rate of occurrence of false negatives and serve as a good surrogate for Cl detection when the effect of transport on the Na-to-Cl ratio is fully understood. The performance of surrogate measurement of Cl by K and Mg, on the other hand, needs to be improved for obtaining more information about that component of sea salt deposition on the canister, and thus to even better understand matrix effect of LIBS detection and the process of Cl-induced corrosion. For future work, surrogate measurement of Cl concentration on SS surfaces by alkali element detection will be integrated into fiber-coupled LIBS with compact devices for field measurement at DCSS facilities. While the difficulty of transmitting high-power laser pulses through optical fibers is noted, direct Cl measurement through fiber-coupled LIBS at low concentration is still highly valuable and may be partially addressed by use of double-pulse excitation.

References

[1] T.M. Ahn, An Approach to Model Abstraction of Stress Corrosion Cracking Damage in Management of Spent Nuclear Fuel and High-Level Waste, ASME 2013 Pressure Vessels and Piping Conference, American Society of Mechanical Engineers. 2013, PVP2013-97139.

[2] S. Eto, T. Fujii, Laser-induced breakdown spectroscopy system for remote measurement of salt in a narrow gap, Spectrochim. Acta B At. Spectrosc. 116 (2016) 51–57.

[3] M. Wataru, H. Kato, S. Kudo, N. Oshima, K. Wada, H. Narutaki, Measurement of Atmospheric Sea Salt Concentration in the Dry Storage Facility of the Spent Nuclear Fuel, 14th International Conference on Nuclear Engineering, American Society of Mechanical Engineers. 2006, pp. 857–863.

[4] S. Eto, J. Tani, K. Shirai, T. Fujii, Measurement of concentration of chlorine attached to a stainless-steel canister material using laser-induced breakdown spectroscopy, Spectrochim. Acta B At. Spectrosc. 87 (2013) 74–80.

[5] L.J. Radziemski, D.A. Cremers, Handbook of Laser Induced Breakdown Spectroscopy, John Wiley & Sons, West Sussex, England, 2006.

[6] K. Hartig, J. Colgan, D. Kilcrease, J. Barefield, II, I. Jovanovic, Laser-induced breakdown spectroscopy using mid-infrared femtosecond pulses, J. Appl. Phys. 118 (2015) 043107.

[7] P. Ko, K. Hartig, J. McNutt, R. Schur, T. Jacomb-Hood, I. Jovanovic, Adaptive femtosecond laser-induced breakdown spectroscopy of uranium, Rev. Sci. Instrum. 84 (2013) 013104.

[8] S. Eto, T. Matsuo, T. Matsumura, T. Fujii, M.Y. Tanaka, Quantitative estimation of carbonation and chloride penetration in reinforced concrete by laser-induced breakdown spectroscopy, Spectrochim. Acta B At. Spectrosc. 101 (2014) 245–253.

[9] E. Tognoni, V. Palleschi, M. Corsi, G. Cristoforetti, Quantitative micro-analysis by laser-induced breakdown spectroscopy: a review of the experimental approaches, Spectrochim. Acta B At. Spectrosc. 57 (2002) 1115–1130.

[10] K. Hartig, J. McNutt, P. Ko, T. Jacomb-Hood, I. Jovanovic, Pulse chirp effects in ultrafast laser-induced breakdown spectroscopy, J. Radioanal. Nucl. Chem. 296 (2013) 135–141.

[11] V. Detalle, M. Sabsabi, L. St-Onge, A. Hamel, R. Héon, Influence of Er:YAG and Nd:YAG wavelengths on laser-induced breakdown spectroscopy measurements under air or helium atmosphere, Appl. Opt. 42 (2003) 5971–5977.

[12] C. Hanson, S. Phongikaroon, J.R. Scott, Temperature effect on Laser-induced breakdown spectroscopy spectra of molten and solid salts, Spectrochim. Acta B At. Spectrosc. 97 (2014) 79–85.

[13] K. Sugiyama, T. Fujii, T. Matsumura, Y. Shiogama, M. Yamaguchi, K. Nemoto, Detection of chlorine with concentration of 0.18 kg/m3 in concrete by laser-induced breakdown spectroscopy, Appl. Opt. 49 (2010) C181–C190.

[14] J. Riley, M. Tongudai, The major cation/chlorinity ratios in sea water, Chem. Geol. 2 (1967) 263–269.

[15] F. Culkin, R. Cox, Sodium, Potassium, Magnesium, Calcium and Strontium in Sea Water, Deep Sea Research and Oceanographic Abstracts, 13, Elsevier. 1976, pp. 789–804.

[16] C.A. Pio, D.A. Lopes, Chlorine loss from marine aerosol in a coastal atmosphere, J. Geophys. Res.: Atmos. 103 (1998) 25263–25272.

[17] D.R. Hitchcock, L.L. Spiller, W.E. Wilson, Sulfuric acid aerosols and HCl release in coastal atmospheres: evidence of rapid formation of sulfuric acid particulates, Atmos. Environ. (1967) 14 (1980) 165–182.

[18] M.M. Tan, S. Cui, J. Yoo, S.-H. Han, K.-S. Ham, S.-H. Nam, Y. Lee, Feasibility of laser-induced breakdown spectroscopy (LIBS) for classification of sea salts, Appl. Spectrosc. 66 (2012) 262–271.

[19] L. Sun, H. Yu, Correction of self-absorption effect in calibration-free laser-induced breakdown spectroscopy by an internal reference method, Talanta 79 (2009) 388–395.

[20] L. Zheng, S. Niu, A.Q. Khan, S. Yuan, J. Yu, H. Zeng, Comparative study of the matrix effect in Cl analysis with laser-induced breakdown spectroscopy in a

pellet or in a dried solution layer on a metallic target, Spectrochim. Acta B At. Spectrosc. 118 (2016) 66–71.

[21] C.R. Bryan, D.G. Enos, Understanding the Environment on the Surface of Spent Nuclear Fuel Interim Storage Containers (No. SAND2013-8487C), Technical Report, Sandia National Laboratories (SNL-NM), Albuquerque, NM (United States), 2013.